Does a dipole mode really exist in the South Atlantic Ocean?

Hyacinth C. Nnamchi,[1,2,3] Jianping Li,[1] and Raymond N. C. Anyadike[3]

Received 1 January 2011; revised 17 April 2011; accepted 11 May 2011; published 4 August 2011.

[1] This study investigates the existence of a dipole mode in the sea surface temperatures (SST) over the South Atlantic Ocean (SAO), using observational and reanalysis data sets from 1950 to 2008. Our results demonstrate that an opposite SST mode, the SAO dipole (SAOD) occurs in the SAO as the anomalous surface waters in the northeastern part; that is, the Atlantic Niño sector and the southwestern part off the Argentina-Uruguay-Brazil coast are consistently anticorrelated in all months. A typical SAOD episode has a life cycle of about eight months, although the peak intensity in which the SST anomalies are evidently coupled to atmospheric circulation and precipitation anomaly fields lasts for four months during the austral winter (May–August). This coupled atmosphere-ocean interaction mechanism appears to be unique, distinct from the classical Atlantic Niño and independent of the direct influence of the Pacific Ocean-based El Niño or global SST variability. The SAOD may provide a useful framework for investigating climate variability and for improved predictions especially over parts of Africa and the Americas, and some preliminary results are already indicated, e.g., the SAOD is widely related to precipitation anomalies in these regions particularly during the austral winter.

Citation: Nnamchi, H. C., J. Li, and R. N. C. Anyadike (2011), Does a dipole mode really exist in the South Atlantic Ocean?, *J. Geophys. Res.*, *116*, D15104, doi:10.1029/2010JD015579.

1. Introduction

[2] As a result of the continuous exchange of heat, moisture, and momentum between the oceans and the atmosphere, variabilities of these two components of the climate system are often coupled and play vital roles in influencing regional and global climate modes. The El Niño–Southern Oscillation (ENSO) [*Bjerknes*, 1969] is the best known example worldwide of coupled ocean-atmosphere interactions causing near global-scale climate anomalies. In addition, however, recent studies have also explored the existence of dipole modes in the various ocean basins and their applications for climate studies.

[3] The Indian Ocean dipole (IOD) has particularly received a lot of attention in recent years. *Saji et al.* [1999] demonstrates that the IOD events are associated with large-scale changes in the equatorial Indian Ocean that has been related to precipitation anomalies in several locations including East Asia [*Guan and Yamagata*, 2003], Sri Lanka [*Lareef et al.*, 2003], India [*Ashok et al.*, 2001; *Ajayamohan and Rao*, 2008], and Australia [*Ashok et al.*, 2003]. With respect to the Atlantic Ocean, the tropical dipole-like mode, also referred to as tropical Atlantic meridional or interhemispheric gradient, which manifests itself as an anomalous asymmetrical structure in the sea surface temperature (SST) field about the Equator associated with a cross-equatorial circulation has been a subject of considerable research [*Weare*, 1977; *Servain and Legler*, 1986; *Servain*, 1991; *Chang et al.*, 1997; *Enfield et al.*, 1999; *Li*, 2001; *Melice and Servain*, 2003; *Chiang and Vimont*, 2004]. This mode has long been linked to regional climate variabilities, for example, precipitation anomalies in the Sahel and the Brazilian Nordeste [*Servain*, 1991].

[4] Geographically located between the Indian and North Atlantic oceans, the South Atlantic Ocean (SAO) is of key significance in local and regional climate variability. Its roles in transporting energy toward the equator via thermohaline circulation as a part of the global ocean conveyor belt and possible impacts on the Northern Hemisphere climates have been highlighted [*Gordon*, 1986; *Weijer et al.*, 2002; *Sterl and Hazeleger*, 2003]. Therefore, improved understanding of the ocean-atmosphere interactions in the SAO is imperative for investigating regional climate variability and for successful prediction over the surrounding regions [see *Goddard and Mason*, 2002; *Trzaska et al.*, 2007].

[5] An aspect of the ocean-atmosphere variability in the SAO that remains unclear is the existence of a dipole mode and its possible connections to the regional climates. While some observational studies [e.g., *Venegas et al.*, 1996, 1997] suggest that a dipole is the dominant mode of coupled variability in the SAO, others [e.g., *Sterl and Hazeleger*, 2003] produced seemingly contradictory results indicating that a dipole mode does not really exist in the basin. The pioneering work of *Venegas et al.* [1996] examined monthly SST and sea level pressure (SLP) data sets from the *Woodruff et al.*

[1]State Key Laboratory of Numerical Modelling for Atmospheric Sciences and Geophysical Fluid Dynamics, Institute of Atmospheric Physics, Chinese Academy of Sciences, Beijing, China.
[2]Graduate University of the Chinese Academy of Sciences, Beijing, China.
[3]Department of Geography, University of Nigeria, Nsukka, Nigeria.

0148-0227/11/2010JD015579

[1987] archive from 1953 to 1992. The first coupled mode identified by the singular value decomposition (SVD) of the anomalies of the two fields accounting for 63% of the total squared covariance was described as oscillation in the strength of the subtropical anticyclone, accompanied by fluctuations of a north–south dipole structure in the SST field.

[6] In a modeling study, *Haarsma et al.* [2003] reported significant atmospheric response to dipole-like SST pattern. Using the SPEEDY (Simplified Parameterizations, primitivE-Equation DYnamics) numerical model forced with a dipole-like SST anomaly (SSTA) during the austral summer months of January to March, *Haarsma et al.* [2003] found strong impacts on atmospheric circulation in the SAO characterized by a deep baroclinic response over the equatorward pole and a shallow equivalent barotropic response over the poleward pole. A number of other studies also obtained dipole-like SSTA in the SAO patterns by subjecting numerical model outputs to the eigen-based techniques such as the empirical orthogonal functions (EOFs) with varimax rotation [*Colberg and Reason*, 2007] and the SVD analyses [*Haarsma et al.*, 2005; *Trzaska et al.*, 2007]. One pole of the dipole is located in the southern part of the SAO off the coast of Argentina, and the other is in the northern part off the coast of West Africa, where the well-known equatorial mode or the so-called Atlantic Niño also occurs [*Zebiak*, 1993; *Latif and Grötzner*, 2000; *Joly and Voldoire*, 2010].

[7] However, one question that remains unresolved relates to whether the apparent SST dipole-like structures reported in these studies represent physical variability in the SAO. This question was first raised by *Sterl and Hazeleger* [2003] as they applied both the EOF and SVD analyses to the SLP and SST data sets over the SAO sector. They identified the first EOF of the SST as consisting of a monopole and the second as consisting of a dipole, but they pointed out that the latter was likely an artifact of the EOF technique [*Dommenget and Latif*, 2002]. Thus, while the first SVD pattern of the coupled SST/SLP obtained by *Sterl and Hazeleger* [2003] apparently has a dipole-like structure, they matched it with the first EOF (i.e., the homogenous mode) and, by also matching the second SVD with the second EOF mode, they described the apparent dipole-like SST pattern as an artifact of the analysis techniques.

[8] Indeed, several studies have argued that the eigen-based methods used in the previous studies to determine the dominant modes of SAO variability often produce artifacts or merely statistical instead of the real climate modes [e.g., *Dommenget and Latif*, 2002; *Compagnucci and Richman*, 2008; *Monahan et al.*, 2009]. Thus, we are still faced with some fundamental questions on the existence of a dipole mode in the SAO and its possible relevance. First, does a dipole mode really exist in the SAO? That is; does warming in the northern part of the SAO occur simultaneously with cooling in the southern part? Second, if so, is there any connection between the dipole mode and regional climate anomalies? Here answers to these questions are explored further, taking advantage of the recent improvements in observational SST data sets [*Rayner et al.*, 2006; *Smith et al.*, 2008].

[9] We present in this paper evidence to show that warming in the northeastern part of the SAO does occur concurrently with cooling in the southwestern part and that these patterns are coupled to atmospheric circulation anomalies. We term this mode the SAO dipole (SAOD), show that it is essentially different from the well-known Atlantic Niño and independent of the direct influence of the El Niño or global SST variability, develop an index to measure its strength, and highlight that the SAOD could prove valuable for investigating regional climates especially precipitation variability over parts of Africa and the Americas. The remaining parts of this paper are presented in four sections. Data and methods are described in section 2. This is followed by the detection of the SAOD in section 3 and the description of its evolution and relations in section 4. The paper ends with summary and concluding remarks in section 5.

2. Data and Methods

[10] Monthly data sets on SST, atmospheric circulation fields, and precipitation have been used in this study. The SST data were drawn from the Hadley Center Global Sea Ice and Sea Surface Temperature (HadISST) analysis data set version 2 [*Rayner et al.*, 2006] available at 1° × 1° longitude/latitude grid resolution and the National Oceanic and Atmospheric Administration (NOAA) Extended Reconstructed SST data set (NOAA ERSST) version 3 [*Smith et al.*, 2008] available at 2° × 2° resolution. Obtained from two different institutions, these data sets enable us to demonstrate the consistency of some results-based different observations. We focus on recent years with generally improved global observations: 1950–2006 for the HadISST and 1950–2008 for the NOAA ERSST data sets, respectively.

[11] Other data sets used include the National Centers for Environmental Prediction (NCEP)/National Center for Atmospheric Research (NCAR) reanalysis data set [*Kalnay et al.*, 1996] at 2.5° × 2.5° grids and the version 2 combined precipitation data set from the Global Precipitation Climatology Project (GPCP) [*Adler et al.*, 2003] available at 2.5° × 2.5° global grids. The NCEP/NCAR reanalysis data sets used cover the period from 1950 to 2008, while the GPCP precipitation data set is for 1979–2008.

[12] First, monthly anomalies were computed for each parameter as the difference between the monthly value for each year and the climatological mean value for the month. The EOF method was then used to determine the dominant modes of SST variability in the SAO. Before computing the EOFs, the anomaly time series were standardized by dividing the time series for each grid point by its standard deviation. The SVD [*Bretherton et al.*, 1992] of the cross-covariance matrix between the SST and SLP anomalies was also used to establish the dominant modes of the coupled ocean-atmosphere variability. These formed the basis for further analyses using correlation and compositing techniques.

[13] From the examination of the climatological-mean SST and SLP data sets (not shown), we noticed that the meteorological equator (the axis of warmest SST coincident with weakest SLP) actually lies north of latitude 0°. Thus, the northern boundary of the SAO is delineated along this axis (i.e., latitude 5°N) so that the domain for computing the EOF and SVD is determined as: 5°N–45°S, 20°E–60°W for the period 1950–2008. While the earlier studies applied these methods, we have changed the spatial domain, period and data sets in the present study to obtain more pronounced opposite polarity. Furthermore, an index of the dipole, defined as the normalized difference between the two polarities of the

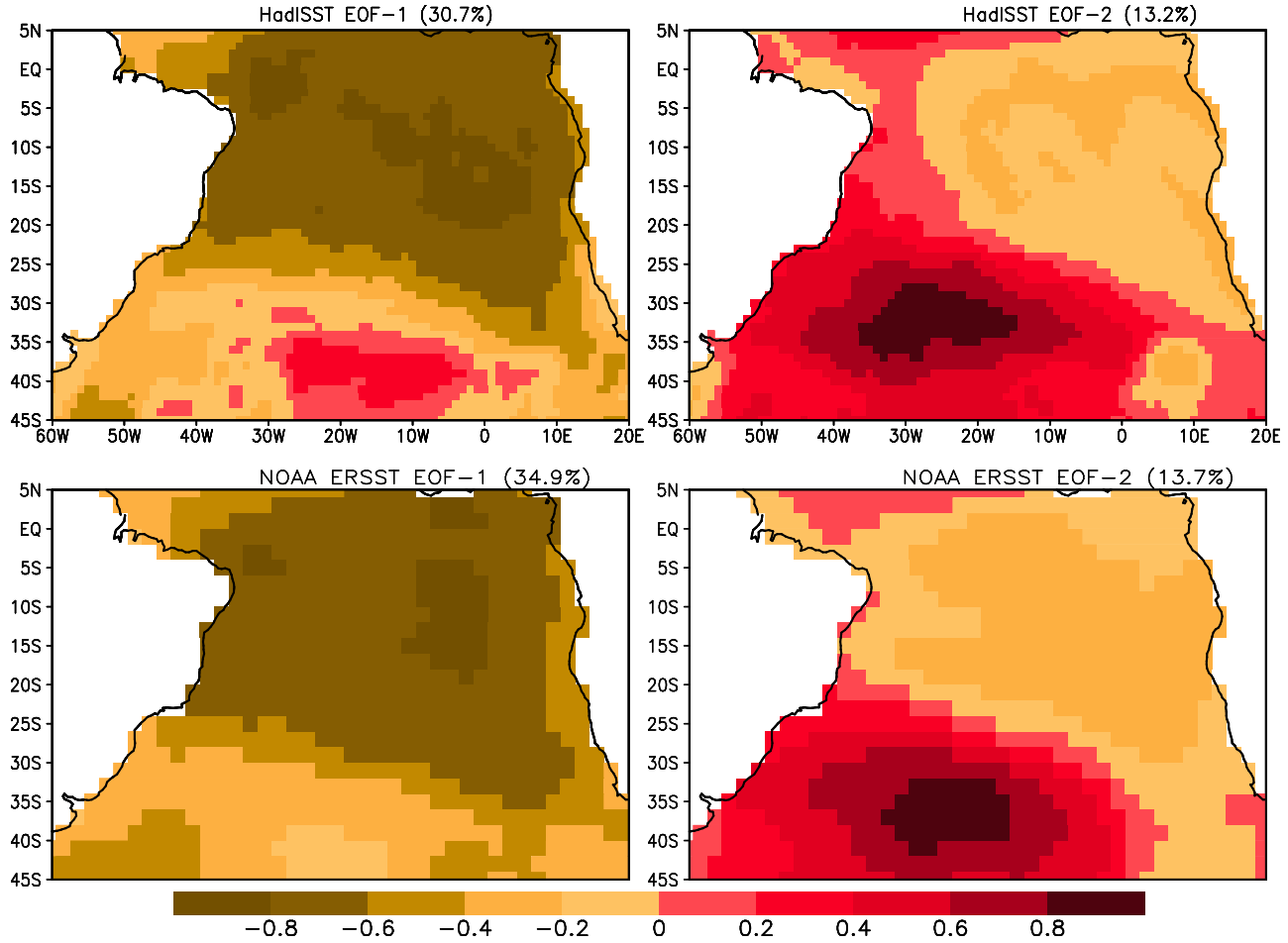

Figure 1. Spatial patterns of the first two EOF modes of SSTA in the SAO based on the (top) HadISST (January 1950 to December 2006) and (bottom) NOAA ERSST (January 1950 to December 2008) data sets.

dipole mode according to *Li and Wang* [2003], was then derived by replicating the SSTA pattern characteristic of the SAOD identified by the SVD. Our particular interest has been on confirming the existence of the SAOD as an independent physical mode of variability and demonstrating that it is different from the classical Atlantic Niño. Unlike the earlier studies, we also analyzed seasonally averaged data sets based on a four-season division of the year and investigated the life cycle of the SAOD.

3. Detection of the SAOD

3.1. Spatial Patterns of the EOF and SVD Analyses

[14] Figure 1 shows the spatial patterns of the first two EOF modes in the SAO based on both the HadISST and NOAA ERSST data sets. The first mode (EOF-1), which carries more than 30% of the total variance in each of the two data sets, is characterized by strong eigenvector loadings in the northern parts of the SAO (north of 25°S). On the other hand, weaker loadings, which degenerate to a different sign in the HadISST data set, characterize the southern part. This pattern is largely reproduced in the NOAA ERSST except that the sign remains the same throughout the domain.

[15] The EOF-2 is characterized by a dipole-like SSTA structure in both data sets. One pole centered at 35°S, 35°W is located in the southwestern domain of the SAO off the Argentina-Uruguay-Brazil coast, while the other pole is in the northeastern part with its center at approximately 10°S, along the Greenwich Meridian off the coast of Central Equatorial Africa (CEA)/West Africa. These are referred to as the southwest pole (SWP) and northeast pole (NEP), respectively, hereafter. The opposing polarity that characterizes this mode indicates that the mechanism of warming of the surface waters off the coast of the CEA/West Africa is associated with concurrent cooling off the Argentina-Uruguay-Brazilian coast, and vice versa. We term this mode the SAO dipole (SAOD) and conduct further analyses to demonstrate its major characteristics and possible relevance.

[16] The EOF analysis is repeated using seasonally averaged HadISST SSTA data sets, and the results show that the major spatial features of the SST variability obtained using the monthly data sets are stable. Thus, EOF-1 is characterized by a uniform pattern in a larger part of the SAO with a seemingly different pattern in the central southern extremity of the study domain in all the seasons (not shown). Similarly, the EOF-2 is characterized by opposite dipole-like

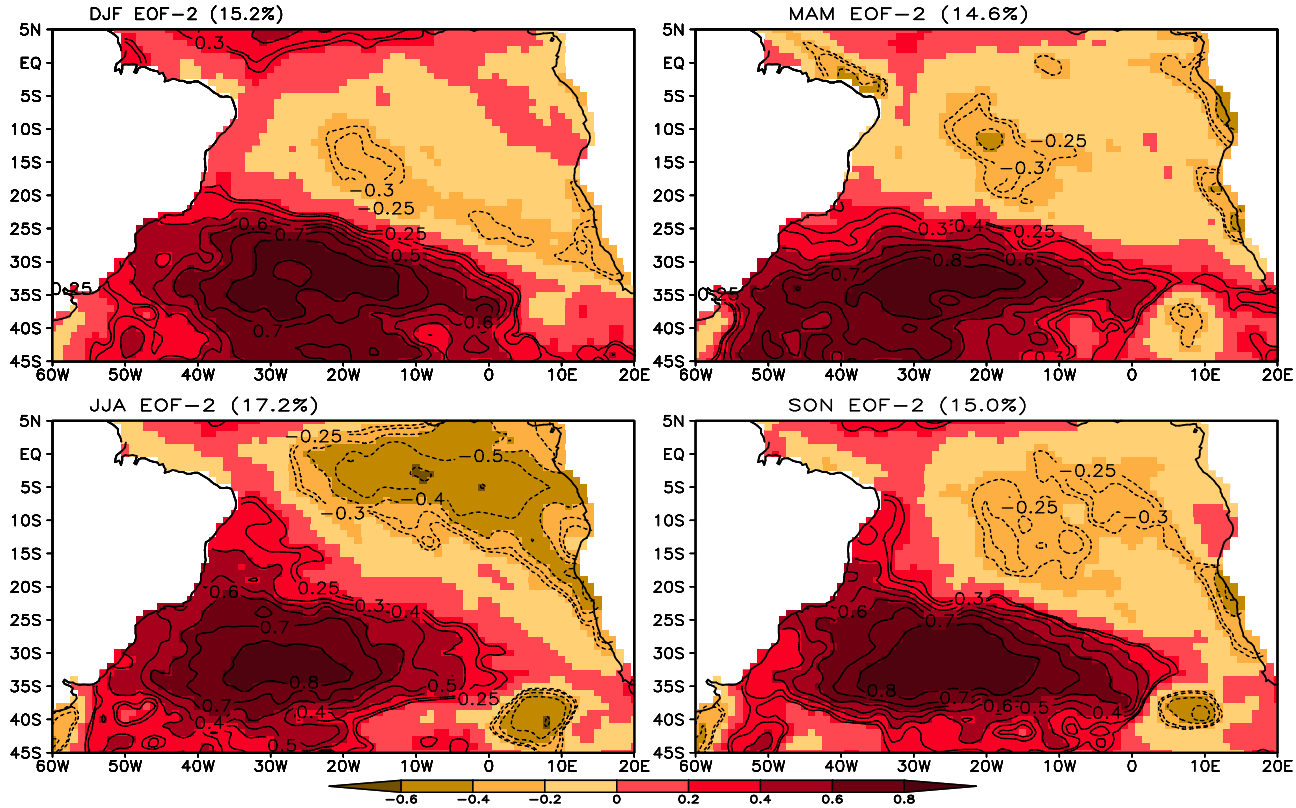

Figure 2. Spatial patterns of EOF-2 of the seasonally averaged SSTA in the SAO based on the HadISST (1950–2006). Contours indicate eigenvectors significant at 95% confidence level based on *t* test. The fractional variance of each EOF mode (in percent) is included in parentheses.

polarity in all the seasons (Figure 2). However, it is readily evident that both the strength and spatial spread of the SAOD undergo marked changes from one season to another. Thus, the NEP is located most southerly in December-January-February (DJF) when it also appears to be comparatively weak. At this time, the SWP extends well southward to the limit of the study domain. By March-April-May (MAM), the NEP extends northward. In June-July-August (JJA), the NEP intensifies further and the center of the SWP is also strongly defined. The NEP appears to weaken again in September-October-November (SON). Hence, the opposite SST polarity that defines the SAOD appears to be best developed during the austral winter.

[17] Figure 3a shows the first mode of the coupled variability of the ocean-atmosphere in the SAO sector determined by the SVD of the anomalies of the monthly SST and SLP. It can be seen that when the ocean and atmosphere are considered together, the first mode becomes the SAOD. This result is basically consistent with the earlier analyses [*Venegas et al.*, 1996, 1997; *Haarsma et al.*, 2005; *Colberg and Reason*, 2007; *Trzaska et al.*, 2007]. In a large measure, the SAOD mode in the present study is also similar to the first SVD mode obtained by *Sterl and Hazeleger* [2003], although they described it as a homogenous pattern.

[18] The centers of the two polarities appear to be best captured in the present study and by *Trzaska et al.* [2007] and are located in the northeastern (i.e., NEP) and southwestern (SWP) parts of the SAO; not merely north-south as was earlier described [*Venegas et al.*, 1996, 1997]. One reason that might be responsible for this kind of spatial pattern is the northward extension of the domain of the SAO to latitude 5°N in the present study and to 10°N in the study by *Trzaska et al.* [2007]. Furthermore, all the above studies (except those by *Venegas et al.* [1996, 1997]) are based on monthly data sets. In the present study, by also analyzing the seasonally averaged SST data sets, it is found that the SAOD undergoes remarkable seasonal changes. This is equally true of the SST/SLP-coupled modes determined by the SVD, which is weakest in austral summer (not shown) and most intense in winter (Figure 3b), and this is reflected in the variances associated with the SAOD vis-à-vis the homogenous mode (Table 1).

[19] From the foregoing, both the EOF and SVD illustrate that the SAOD is best developed during the austral winter. This is inconsistent, however, with the report of *Venegas et al.* [1997] because they investigated the seasonal changes of the first three modes of the SVD of the SAO SST and SLP anomalies based on a two-season division of the year. They defined the austral winter as May to October and the summer as November to April, and they showed that the coupling of the dipole (and indeed other modes) was most significant during summer. However, *Venegas et al.* [1997] described that result as "surprising," pointing out that the seasonality exhibited in the coverage of the Comprehensive Ocean–Atmosphere Data set [*Woodruff et al.*, 1987] may partly account for the stronger coupling in summer. The SST data

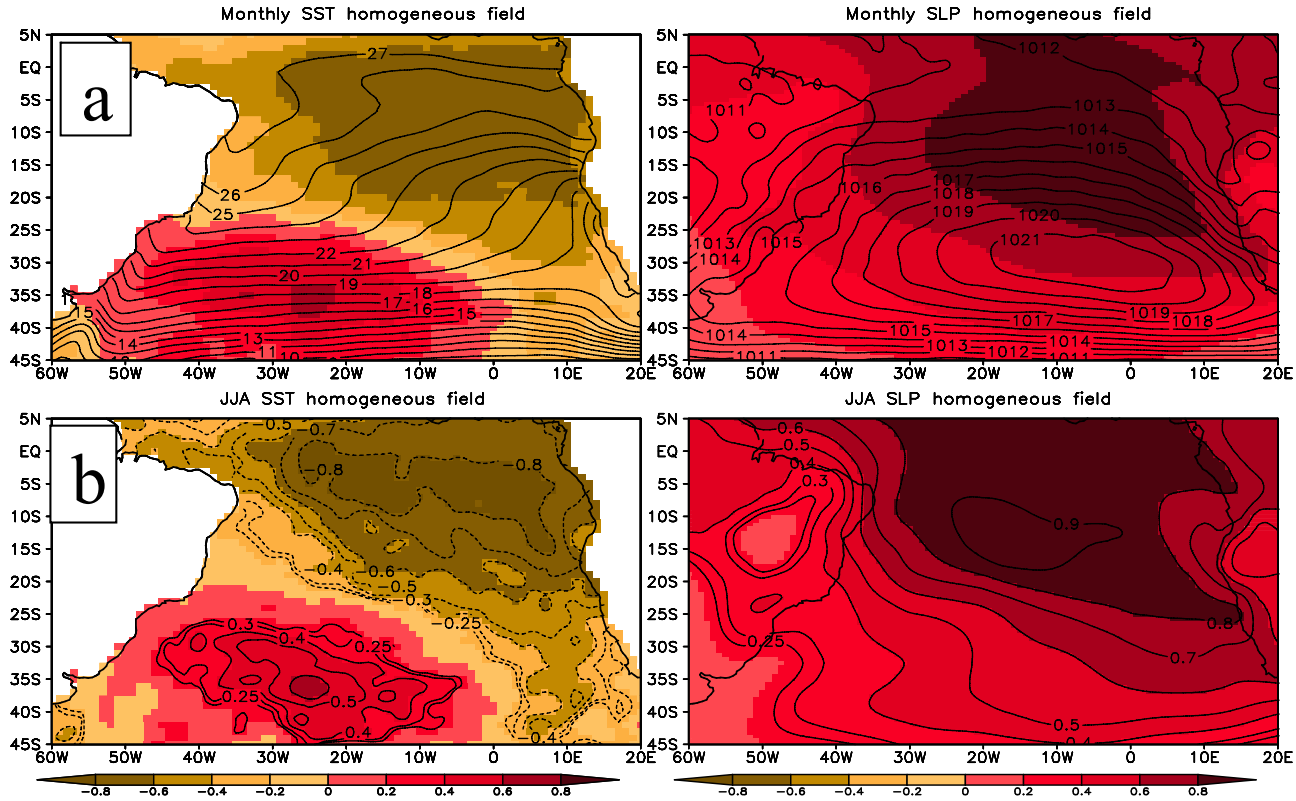

Figure 3. (a) Spatial patterns of the first SVD of the monthly anomalies of (left) SST and (right) SLP in the SAO based on the HadISST and NCAR/NCEP reanalysis (1950–2006). Contours show the climatological mean SST and SLP. (b) Same as Figure 3a except for JJA-averaged data sets. Contours indicate loadings significant at 95% based on *t* test.

sets used in the present study [*Rayner et al.*, 2006; *Smith et al.*, 2008] are based on recently updated archives and do not have such pronounced seasonal bias; this improvement appears to be reflected in the above results.

3.2. SST Variability of the NEP and SWP

[20] In this section, we demonstrate that the SST variability of the NEP and SWP really evolve in an opposing fashion. In defining the boundaries of the two polarity domains, we aimed to use a combination of their time series to reproduce the SAOD-type SSTA obtained by the SVD. Because the SSTA associated with the SAOD represents large-scale variability in the SAO basin, the boundaries of the NEP and SWP are defined over large domains to capture large-scale dynamics, i.e., the NEP is delineated as 10°E–20°W, 0°S–15°S, while the SWP is defined as 10°W–40°W, 25°S–40°S (Figure 4). An index of the SST variability in each domain is determined as the domain-averaged SSTA within it. Thus, we have two index time series from the NEP and SWP as follows: $SSTA_{NEP}$ and $SSTA_{SWP}$.

[21] Here our basic assumption is that, if a dipole mode really exists in the SAO, then the NEP and SWP time series should evolve in an opposing manner. This assumption is then tested by computing the detrended correlation between the $SSTA_{NEP}$ and $SSTA_{SWP}$ time series first using the seasonally averaged data (Table 2). Interestingly, all the correlation coefficients are negative and significant based on the *t* test. This means that, indeed, warming of the surface waters over the NEP does occur concurrently with cooling over the SWP and vice versa. However, from Table 2 the correlation for the JJA for which we have noted from the EOF and SVD analyses that SAOD is best developed is not remarkably different from the other seasons. The same could be said of the correlation between the monthly time series of $SSTA_{NEP}$ and $SSTA_{SWP}$, which is strongest in March and October and weakest in April (Figure 5a). More importantly, however, robust negative correlations are found between the two time series in all the months.

[22] In order to examine the interdecadal relationship between the $SSTA_{NEP}$ and $SSTA_{SWP}$, their correlation over a 15 year running window has also been computed (Figure 5b). A common feature of the correlation plots is the occurrence of positive correlation during the 1960–1970 decade for all the seasons. This is most noticeable in JJA and at least partly explains why the correlation of the entire series (Table 2 and Figure 5a) is not as strong as would be expected from the

Table 1. Squared Covariance (SC) and Correlation Coefficient of the SST and SLP Expansion Coefficient Associated With SVD the Dipole Mode

	Months	DJF	MAM	JJA	SON
SC (%)	47.74	29.44	47.51	64.26	46.8
Correlation[a]	−0.42	−0.61	−0.65	−0.69	−0.61

[a]All correlation coefficients are significant at the 95% confidence level.

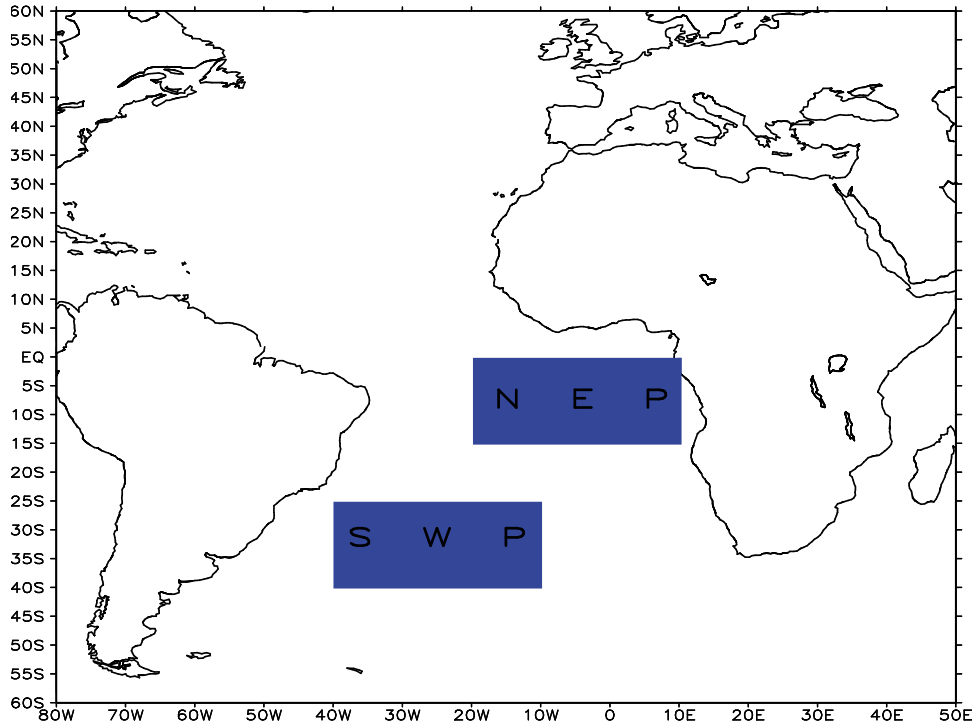

Figure 4. Location of the NEP (10°E–20°W, 0°S–15°S) and SWP (10°W–40°W, 25°S–40°S) used for defining the SAODI.

results of the EOF and SVD analyses, as well as the composites described later in section 4. This pattern possibly relates to the interdecadal variability of the SAOD; while the general tendency is opposite polarity, there are also periods during which the two domains are characterized by a uniform SST pattern. This is also highlighted by the fact that the first EOF mode of the SSTA is dominated by a domain-wide homogeneity.

3.3. Definition of the SAOD Index (SAODI)

[23] We present a measure of SAOD events that could be used for investigating its strength and connections to larger-scale climate variability. Indices derived from oceanic variables are a useful measure for describing climate variability, particularly because the ocean has a long memory and will therefore provide a reliable representation of SAOD events. To derive an index of the SAOD, we consider the first two EOF modes of SST variability in the SAO and compare the index obtained with the SVD result. As shown earlier, the first mode of SST variability in the SAO is largely homogeneous (H) and the second mode is a dipole mode (D). The dipole mode may be further separated into two parts, namely, the dipole for the NEP (D_N) and for the SWP (D_S). Therefore, the SST variability of the two poles may be described by the following relations:

$$\mathrm{SSTA_{NEP}} = H + D_N \quad (1)$$

$$\mathrm{SSTA_{SWP}} = H + D_S \quad (2)$$

The normalized difference between the two equations: equation (1) minus equation (2), cancels the homogeneous component so that we are left with only $D_N - D_S$. This yields a measure the how the NEP warms relative to the cooling of the SWP, and consequently indicates the magnitude of SAOD events. Therefore, the SAOD index (SAODI) is defined as the normalized difference in SSTA between the NEP and SWP. Positive (negative) values of the SAODI indicate warming (cooling) in the NEP off the coast of CEA/West Africa and cooling (warming) in the SWP off the Argentina-Uruguay-Brazil coast.

[24] The SAODI is presented graphically with the SSTA time series of the SVD-1 as a normalized anomaly series based on the HadISST data set (Figure 6a). The SAODI effectively represents SAOD events as shown by its one-to-one correspondence with the SVD-1 time series (for n = 684, correlation = 0.93). We have also computed the correlation maps of the SAODI and SVD-1 time series with SSTA in the SAO sector (Figure 6b). Again, we see that the new index adequately captures the main spatial features of the SAOD, i.e., a reversal in sign between the two distinctive poles with strong SSTA patterns, one centered on the SWP and the other centered on the NEP. For the four seasons also, the SAODI

Table 2. Coefficients of Detrended Correlation Between the $\mathrm{SSTA_{NEP}}$ and $\mathrm{SSTA_{SWP}}$

		Season			
Data Set	Months	DJF	MAM	JJA	SON
ERSST	−0.29[a]	−0.31[a]	−0.31[a]	−0.30[a]	−0.38[a]
HadISST	−0.27[a]	−0.35[a]	−0.20[b]	−0.33[a]	−0.29[a]

[a]95% significance based on the t test.
[b]90% significance based on the t test.

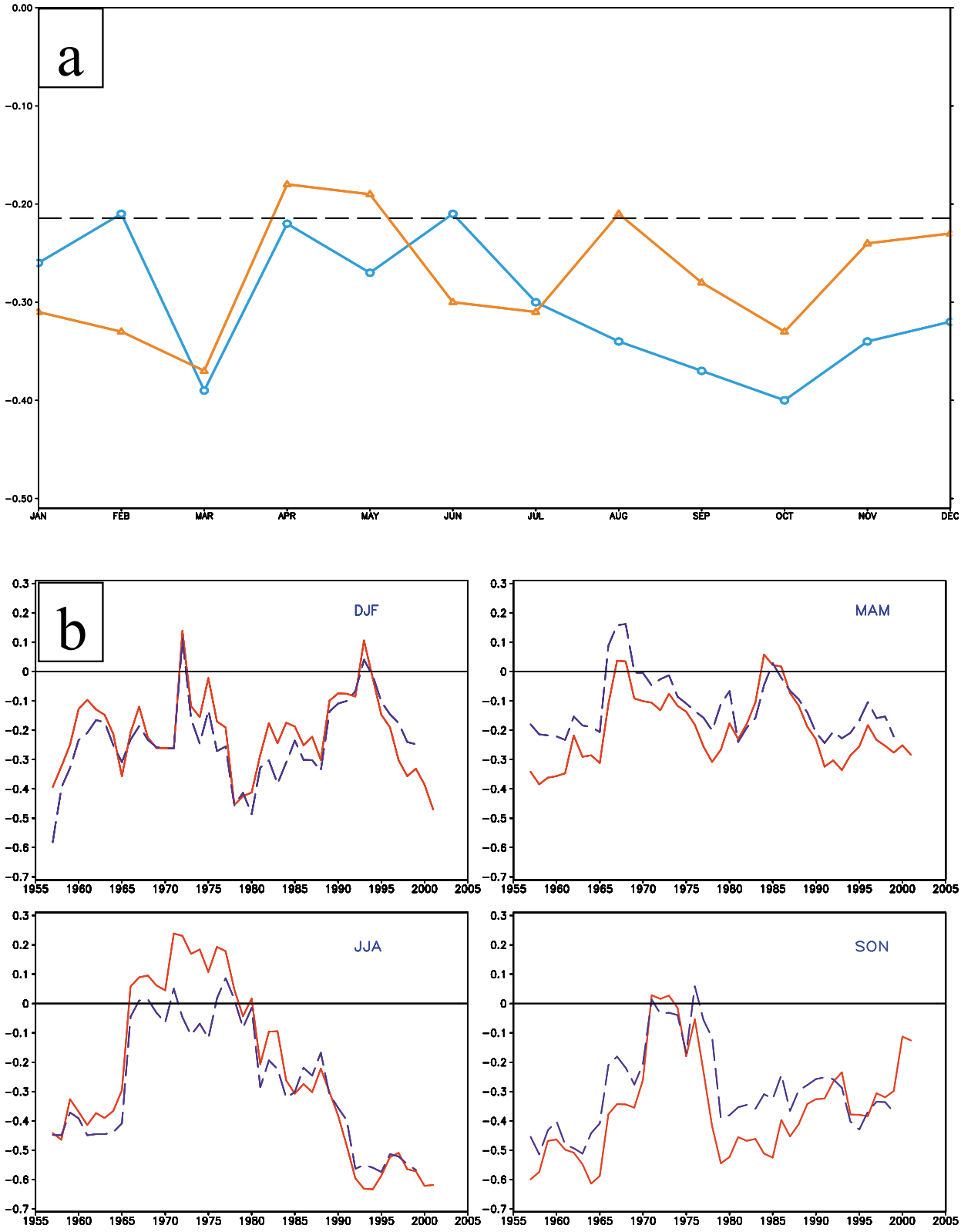

Figure 5. (a) Simultaneous correlation of the monthly $SSTA_{NEP}$ and $SSTA_{SWP}$ based on the HadISST (circular ticks) and NOAA ERSST (triangular ticks) data sets. Dashed line indicates correlation coefficients significant at 90% confidence level based on the *t* test. (b) Fifteen-year sliding correlation between the seasonally averaged values of $SSTA_{NEP}$ and $SSTA_{SWP}$ time series based on the HadISST (dashed line) and NOAA ERSST (solid line) data sets. Both time series were detrended prior to calculating the correlations.

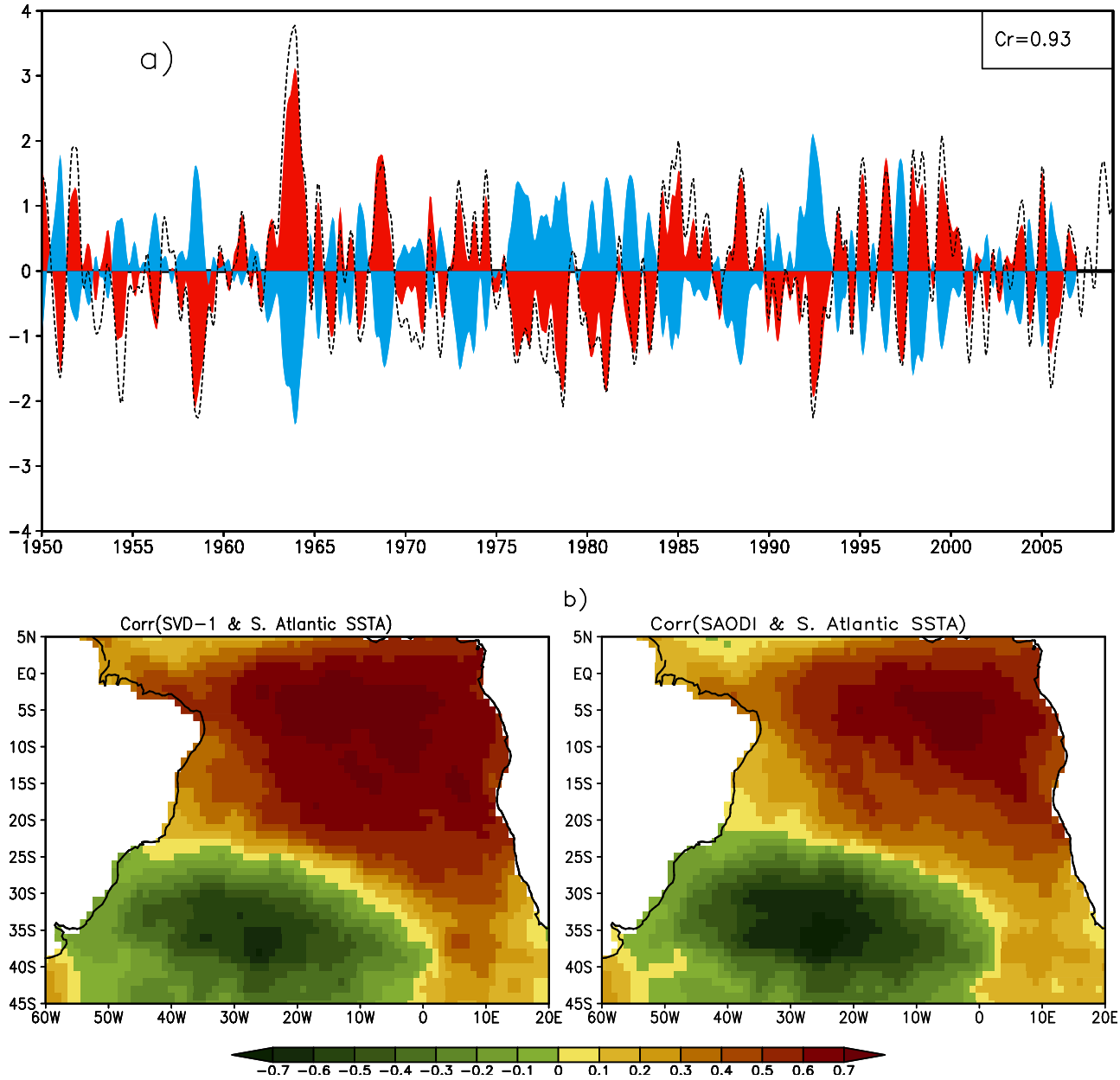

Figure 6. (a) Normalized time series of SVD-1 (blue, inversed for graphical presentation) and the SAODI (red); their detrended correlation coefficient is indicated in the upper right box. Dotted line is the SAODI derived from the NOAA ERSST (1950–2008). All three time series have been smoothed using 7 month Gaussian-type filter. (b) Correlation maps of SVD-1 (Figure 3b, left) and SAODI (Figure 3b, right) with SSTA over the SAO.

effectively reproduces the time series of the associated SVD mode (Figure 7). However, judging by the magnitude of the correlation coefficient between the SAODI and the SVDs, the index best replicates the dipole mode in JJA followed by SON and MAM when their correlation coefficients are very robust (>0.90).

4. Description of the SAOD

4.1. Atlantic Niño Versus the SAOD

[25] The existence of an equatorial zonal mode termed the Atlantic Niño in the tropical South Atlantic Ocean has long been recognized [*Zebiak*, 1993; *Latif and Grötzner*, 2000; *Okumura and Xie*, 2006; *Hu and Huang*, 2007; *Ding et al.*, 2010]. It then becomes imperative to investigate the relationship between this well-known mode and the SAOD. According to *Zebiak* [1993], the Atlantic Niño index or the so-called Atl-3 is defined as the domain averaged SSTA over 3°N–3°N, 0°W–20°W.

[26] The time series correlations among the SAODI, Atl-3, NEP, and SWP are computed using the monthly NOAA ERSST data set (Table 3). The correlations illustrate the relevance of the linear trend coefficient in the variability of these indices; in particular, the correlation between the SWP

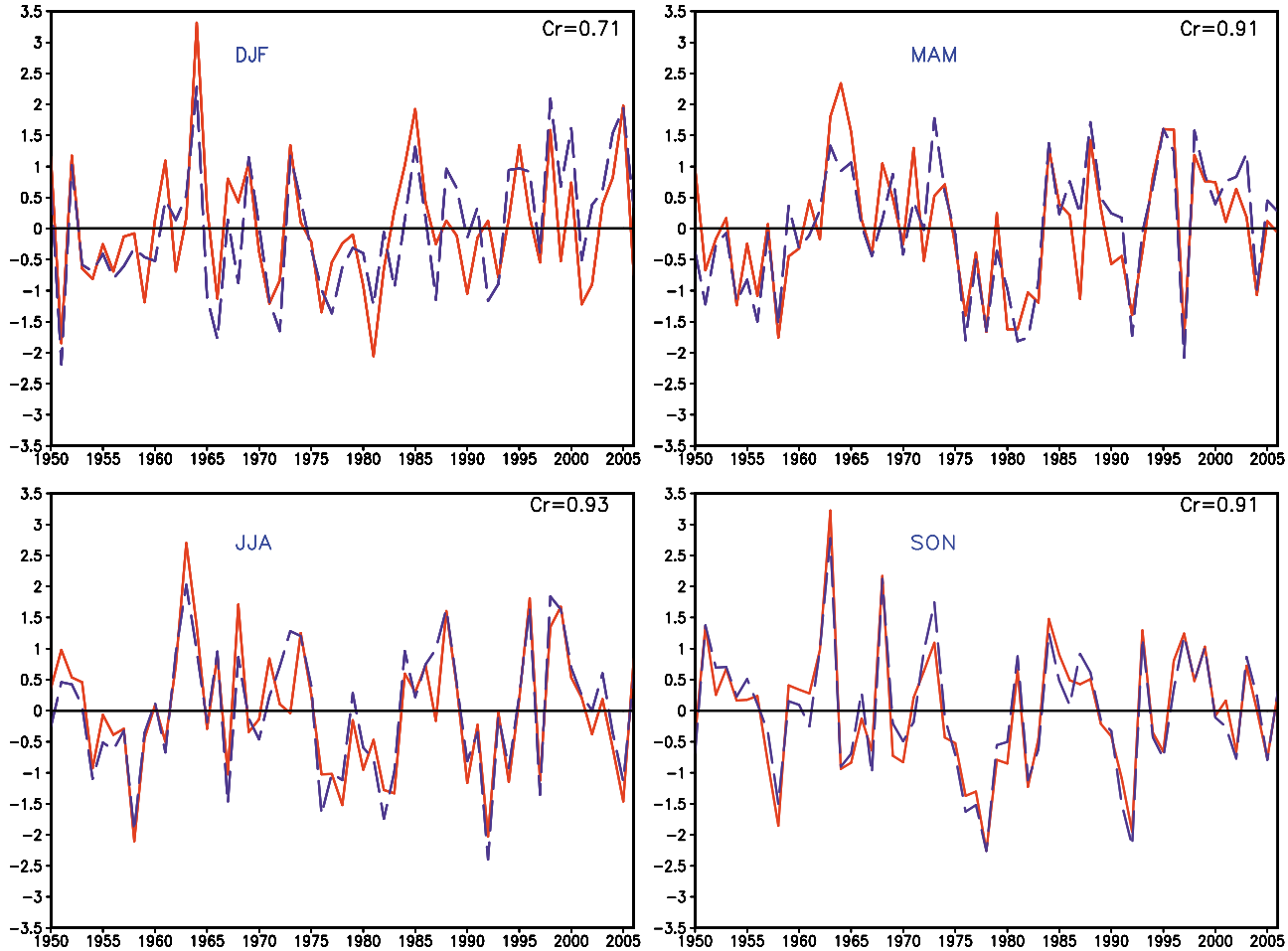

Figure 7. Normalized time series of the seasonal SAODI (solid lines) and the corresponding SVD time series (dashed lines). SVD-1 is the dipole mode in MAM, JJA, and SON, while in DJF the dipole is identified as SVD-2.

and the NEP/Atl-3 become negative (and significant) only after detrending the time series. At this stage, two important issues of interest on the variability of the SAO are readily apparent. First, the Atlantic Niño and SAOD are strongly positively correlated. Second, the intensity of the Atlantic Niño primarily peaks in austral winter [*Zebiak*, 1993], when we have shown in section 3 that the strongest intensity of the SAOD also occurs. These raise fundamental scientific questions on the variability of the SAO: Does the cooling anomaly occur over the SWP off the Argentina-Uruguay-Brazil coast during Atlantic Niño events? Is the SAOD really different from the well-known Atlantic Niño?

[27] In order to demonstrate that the SAOD is a unique mode, distinct from the Atlantic Niño, we focus on JJA when both phenomena are best developed and examine the structures of the SSTA over the SAO for the study period. Figure 8a reveals that some cases of positive Atl-3 index are concurrently associated with negative $SSTA_{SWP}$, while others are not. To illustrate the spatial character of the SSTA during each phenomenon, these indices are used as the basis for compositing. The composite of the Atlantic Niño is based on the normalized Atl-3 index $\geq 0.5°C$ provided that the $SSTA_{SWP}$ for the year $\geq -0.2°C$, while the SAOD composite is based on the co-occurrence of $SSTA_{SWP} \leq -0.5°C$ and Atl-3 index $\geq 0.5°C$.

[28] As shown in Figure 8b two distinct, large-scale SSTA patterns occur in the SAO; one is characterized by pronounced spatially, coherent warming only in the NEP/Atlantic Niño region, and we regard this as the classical Atlantic Niño. The other is defined by significant warming in the Atlantic Niño sector associated with concurrent significant cooling over the SWP off the Argentina-Uruguay-Brazil coast; this represents the SAOD mode. Note that the magnitudes of the SSTA over

Table 3. Coefficients of Correlation Between the Monthly SAOD, Atl-3, $SSTA_{NEP}$, and $SSTA_{SWP}$ Indices Based on the NOAA ERSST Data Set[a]

	SAODI	Atl-3	NEP	SWP
SAODI	1			
Atl-3	0.60(0.70)	1		
NEP	0.67(0.81)	0.92(0.87)	1	
SWP	−0.61(−0.80)	0.18(−0.24)	0.18(−0.29)	1

[a]All detrended coefficients (in parentheses) are significant at 95% confidence level based on the *t* test.

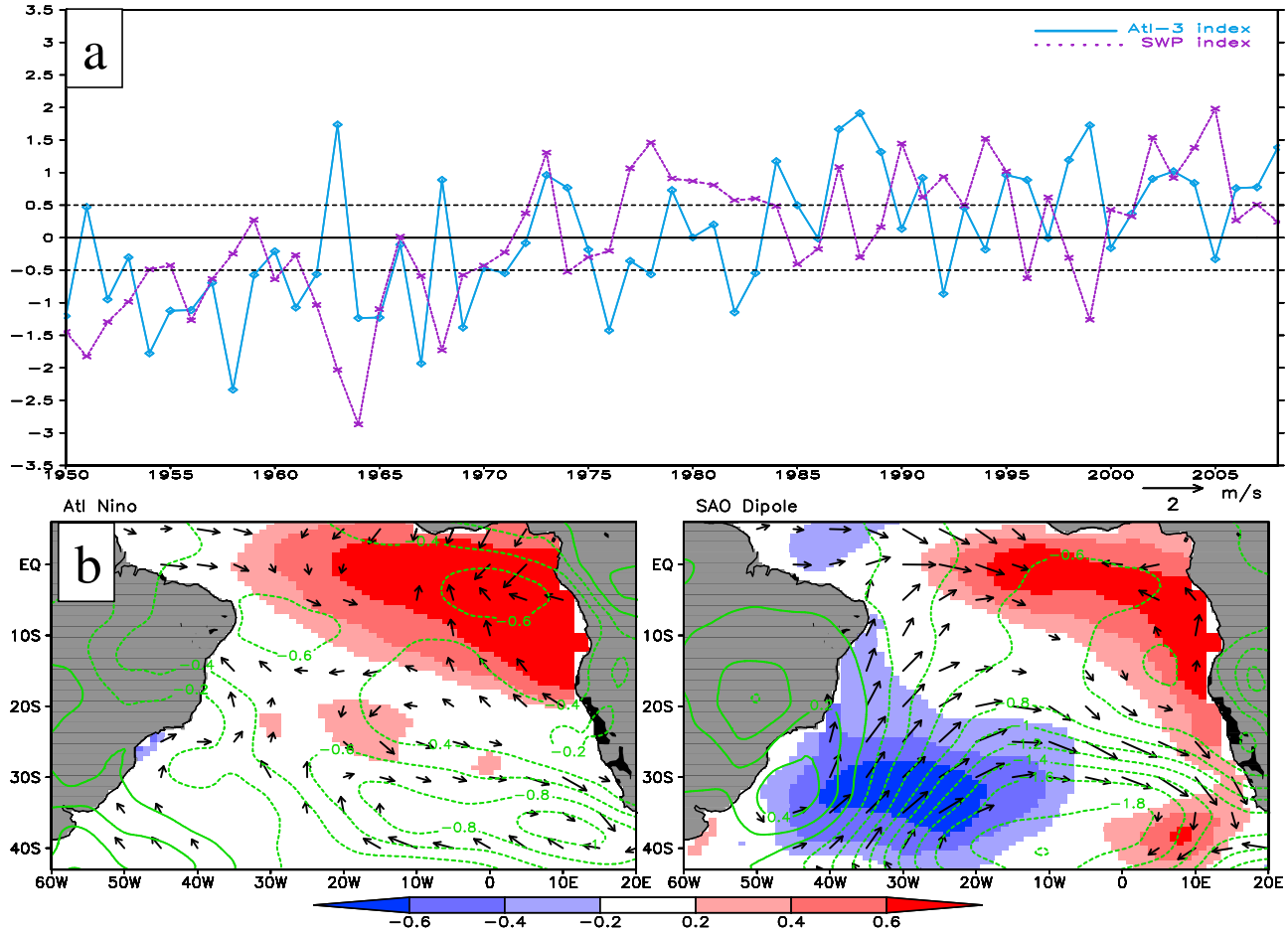

Figure 8. (a) Normalized time series of the JJA averaged Atl-3 index (crossed ticks) and the $SSTA_{SWP}$ (diamond ticks). (b) Composite averages of the SST, surface winds, and SLP anomalies illustrating the classical Atlantic Niño (1984, 1988, 1989, 1998, and 2008) and the SAOD (1951, 1963, 1974, 1996, and 1999). Atlantic Niño composites are based on the normalized Atl-3 index ≥0.5°C provided that the $SSTA_{SWP}$ for the year is ≥−0.2°C; SAOD composites are based on Atl-3 index ≥0.5°C and $SSTA_{SWP}$ ≤−0.5°C. Shading indicates SSTA composites significant at 90% confidence level based on two-tailed *t* test, while the arrows indicate wind anomalies significant at 90% confidence.

the two poles—NEP and SWP—are equally intense and spatially similar but of opposite signs during the SAOD.

[29] The circulation anomalies during SAOD events are characterized by the weakening of the South Atlantic Sub-Tropical Anticyclone (STA; climatologically centered at 30°S, 15°W in JJA) as well as the Atlantic trade winds and intensified equatorial westerlies (Figure 8b). This gives rise to the reversal of the direction of the anticyclonic (i.e., anticlockwise) circulation over the STA. Therefore, climatological southward winds off the Argentina-Uruguay coast exhibit a northward tendency during the SAOD. At the equatorial region these northward winds are deflected to the east to form a part of strong westerly winds that blow toward the NEP. At the NEP, there is a complementing stream of strong northward winds emanating off the CEA coast.

4.2. Evolution of the SST and Surface Wind Anomalies During the SAOD

[30] Using the same SAOD years as in section 4.1, we examine the life cycle of typical SAOD episodes. As shown in Figure 9a, warm SSTA first appears off the coast of Angola, while the southwestern extremity off the coast of Argentina is characterized by developing cooling anomalies in March–April. Anomalous surface winds emanating from the SWP begin to exhibit a northward tendency; this stage may be regarded as the "preonset" of the SAOD.

[31] A dramatically rapid peaking of the SSTA of both polarity domains occurs in May–June, marking the proper onset of the "active phase" of the SAOD. Strong surface winds emanating from the SWP blows northward toward the NEP. This is complemented by southeasterly winds originating off the coast of CEA, leading to convergence over NEP. These patterns intensify further such that the peak intensity of the SAOD occurs in July–August.

[32] However, by September–October the strength and areal extent of the SSTA, particularly over the NEP, become greatly reduced, although the SWP is still quite intense. This stage during which the ocean-atmosphere link between the NEP and SWP breaks down (although the SAOD-type SSTA is still discernable) may be regarded as the "decaying or

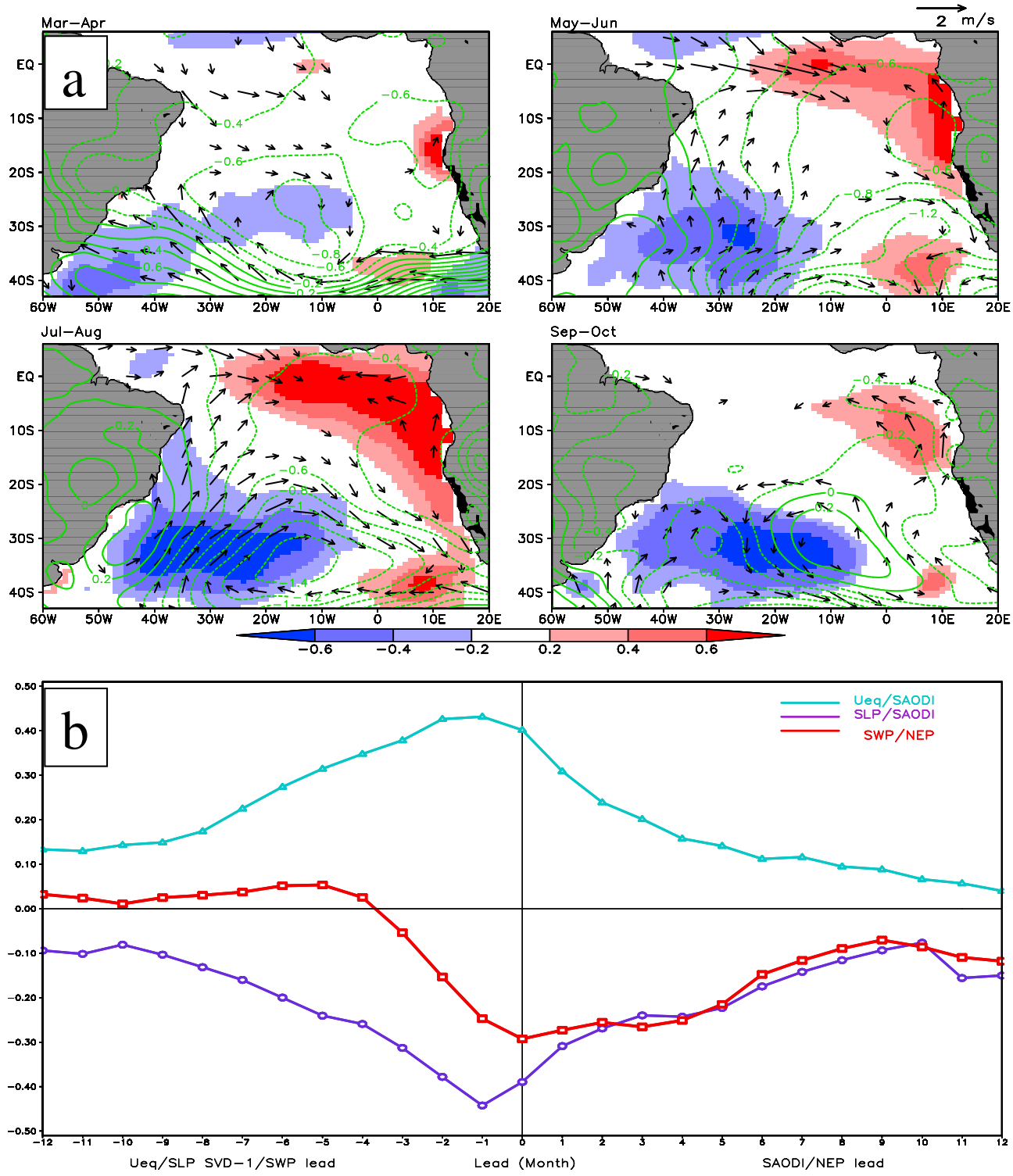

Figure 9. (a) Same as Figure 8b except for the evolution of the SAOD. (b) Cross correlation of the SAODI and SVD-1 time series of the anomalous SLP (circular ticks) and Ueq(triangular ticks) between the $SSTA_{NEP}$ and $SSTA_{SWP}$ times series (square ticks).

weakening phase" of the dipole episode. Note that the warm SSTA in the NEP regions weakens more rapidly compared with the cool SSTA over the SWP during the life cycle of the SAOD, although the precedence in evolution of the NEP/SWP is not immediately clear from cross-correlation analysis (Figure 9b).

[33] Oceanic and atmospheric processes often reinforce each other. This is quite evident during the peak phase of the

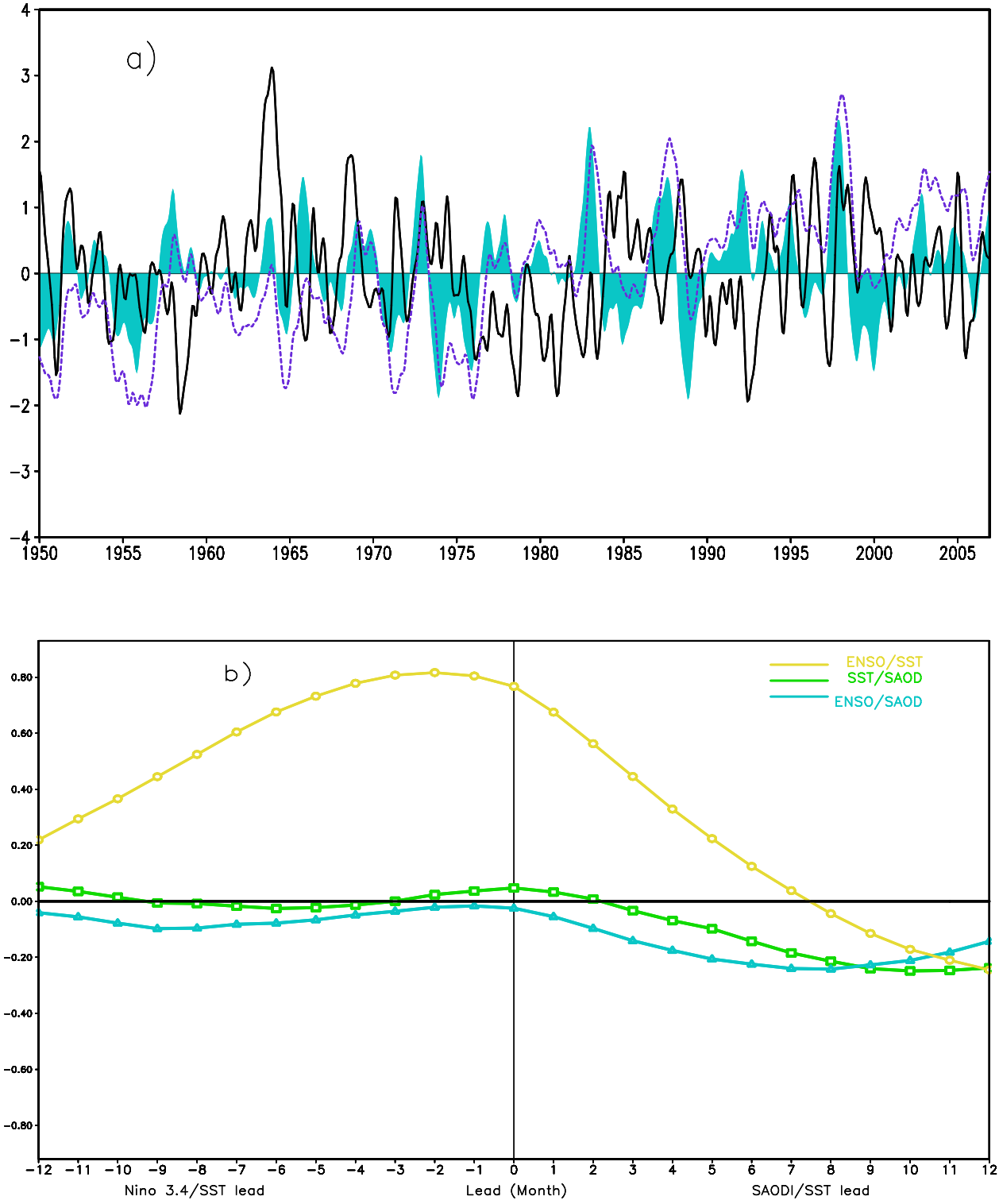

Figure 10. (a) Temporal evolution of the monthly SAODI (solid line), Niño 3.4 index (shading), and EOF-1 time series of global SSTA (dotted line). All three time series have been normalized by their respective standard deviations and smoothed using 7 month Gaussian-type filter. (b) Cross correlations between the Niño 3.4 and EOF-1 of the global SSTA (open circle ticks), the SAODI and Niño 3.4 (triangular ticks), and the SAODI and global SST EOF-1 (open square ticks). All time series were detrended prior to computing the correlations.

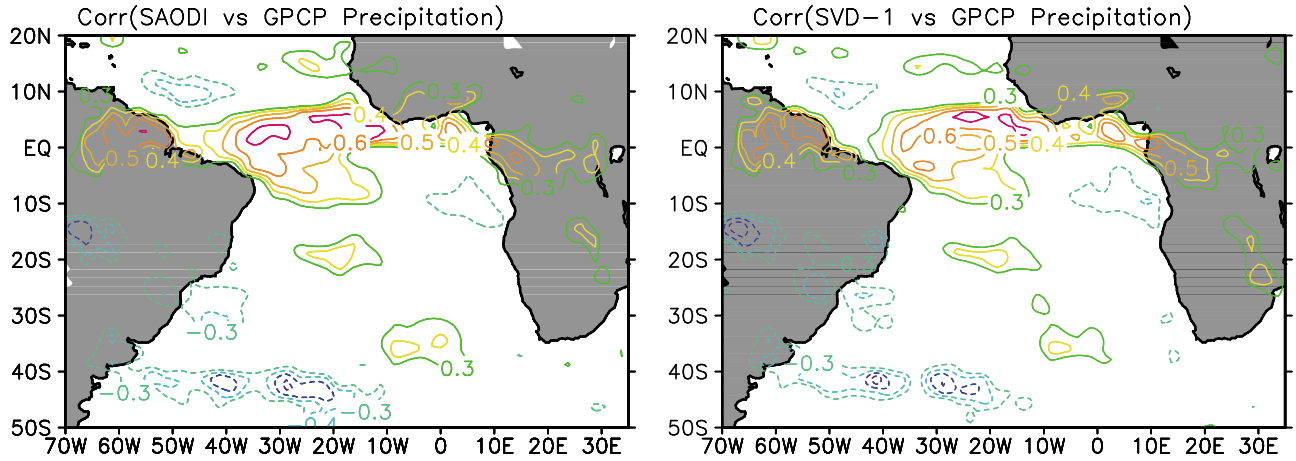

Figure 11. Correlation maps of the (left) SAODI and (right) SST SVD-1 time series with GPCP precipitation anomalies (1979–2008). Only correlation coefficients significant at 95% confidence level based on the *t* test are contoured. Dotted (solid) contours indicate negative (positive) coefficients.

SAOD event. The question then is: Does the SAOD-type SSTA induce or is it induced by the associated atmospheric processes? To investigate this possible cause-and-effect, two atmospheric indices associated with the SAOD are defined as follows: (a) Time series of the SVD-1 of the SLP. This index is strongly correlated with the domain-averaged SLP anomalies over the SAO sector (20°E–60°W; 5°N–45°S) (correlation >0.80). (b) The SAODI is strongly correlated with equatorial winds, particularly the zonal component (not shown). Indeed, the anomalous surface winds emanating from the SWP blow to the NEP via the western segment of the NEP in the equatorial belt. Therefore, we define an equatorial wind index of the zonal wind component (Ueq) associated with the SAOD as the domain averaged anomalies over: 10°W–30°W; 5°N–5°S.

[34] Figure 9b shows that negative antisymmetrical correlation exists between the SAODI and the SVD-1 time series of SLP throughout the 24 month lag. This indicates that positive SAOD events are associated with large-scale negative pressure anomalies in the SAO sector. The correlation is most robust when SLP leads by one month, consistent with the work of *Venegas et al.* [1997]. Similarly, the lagged correlation of SAODI and the Ueq is most robust at when Ueq leads by one month. The positive symmetrical correlation of SAODI with Ueq shows that a strong SAOD episode is associated with the strengthening of the equatorial westerlies.

4.3. SAOD and El Niño

[35] The SAOD appears to be independent of the equatorial Pacific Ocean-based ENSO because there is no simultaneous correlation between the SAODI and Niño indices. However, the superimposition of the Niño 3.4 index on the SAODI (Figure 10a) reveals that some episodes of positive SAOD event coincide with ENSO years (e.g., 1969, 1973, and 1997). Yet positive SAOD events also occur in La Niña years (e.g., 1973, 1984, and 1999).

[36] Figure 10a also shows the relationship between the SAODI and global SST variability represented by the time series of the first EOF-1 mode, which carries 14.8% of the total variance of the global SST variability based on the HadISST monthly data set. As in the case of ENSO, the global SSTA appears to be unrelated to SAOD; there is no simultaneous correlation between SAODI and the EOF-1 time series. On the other hand, the close connection (for n = 684, correlation = +0.77) between the time series of the EOF-1 and Niño 3.4 index highlights the overriding significance of ENSO in global SST variability, which is also very striking in the spatial pattern of EOF-1 of the global SST variability (not shown).

[37] While a direct connection with ENSO is not obvious, we have investigated the possible lagged relationship between the SAODI, Niño 3.4, and the EOF-1 time series (Figure 10b). The results show that the correlation of SAOD and ENSO in the ±24 month lag is most robust (~−0.25) when the SAOD leads by 7–8 months. The lagged correlation of the SAODI and the EOF-1 of the global SST variability exhibits a similar pattern but lags behind the SAODI/ENSO correlation by two months.

4.4. SAOD and Regional Precipitation Anomalies

[38] Our analyses reveal that the SAOD is strongly associated with precipitation anomalies within the SAO and over the nearby Africa and the Americas. However, this relationship is seasonally dependent, being most pronounced during the peak intensity of the SAOD in austral winter. As has been elaborated upon elsewhere [*Nnamchi and Li*, 2011], the occurrence of warming anomalies over the NEP is associated with large-scale convergence and vigorous upward motion and consequently enhanced precipitation. Conversely, the SWP is characterized by subsidence motion and therefore suppressed precipitation during the positive phase of the SAOD.

[39] This is shown by the correlation patterns of regional precipitation anomalies using two indices of the SAOD, namely, the SAODI and SVD-1 time series during the austral winter (Figure 11). The SAOD is significantly positively correlated with precipitation anomalies over the NEP and the nearby equatorial parts of the Americas, CEA, and West Africa. On the other hand, robust negative correlation exists between the SAOD precipitation anomalies over the SWP and the surrounding parts Argentina, Uruguay, Brazil,

Bolivia, and Paraguay. Thus, the opposite polarity in the SST field that occurs during the SAOD is also reflected in the precipitation field.

5. Summary and Concluding Remarks

[40] Based on observational and reanalysis data sets, this paper demonstrates that opposite polarity: the SAOD represents an important mode of coupled air-sea interaction in the SAO. It is identified as the EOF-2 of SSTA based on monthly and seasonally averaged data sets. One center of the SAOD is located in the southwestern domain of the SAO off the Argentina-Uruguay-Brazil coast (the SWP) and the other pole is in the northeast part off the coast of CEA/West Africa (the NEP). The major features of the SAOD are found again by applying the SVD to the SST and SLP anomalies to detect the ocean-atmosphere-coupled variability. SVD analysis shows that the SAOD is the leading mode (i.e., SVD-1). It exhibits marked seasonal changes in intensity, being strongest during the austral winter and weakest in summer.

[41] The correlations of the $SSTA_{NEP}$ and $SSTA_{SWP}$ time series are negative and robust based on monthly and seasonally averaged HadISST and NOAA ERSST data sets. The SAOD mode is the mechanism of warming (cooling) of the surface waters off the coast of the CEA/West Africa associated with concurrent cooling (warming) off the Argentina-Uruguay-Brazil coast. Its index, the SAODI defined as the normalized difference in SSTA between 10°E–20°W, 0°–15°S and 10°W–40°W, 25°S–40°S effectively reproduces the SST pattern associated with the SAOD diagnosed by the EOF, SVD, and composite analyses.

[42] SAOD appears to represent an inherent and unique mode, distinct from the well-known Atlantic Niño in which there are warming anomalies only over the NEP/Atlantic Niño region. It is very weakly correlated with ENSO and global SST variability, even on a lagged time scale, indicating that it may be locally generated. A typical SAOD episode has a life cycle of about eight months, but the active phase in which the SST gradients are strongly linked to the atmospheric circulation and precipitation fields occurs in austral winter, May–August. Associated with the SAOD events are large-scale changes in the surface circulation field characterized by the weakening of the South Atlantic STA, a northward stream of winds emanating from the SWP that, on reaching the equatorial belt, reinforces the dominant anomalous westerlies and blows toward the NEP where it meets a complementing southerly flow emanating off the African coast.

[43] There are some aspects such as the occurrence of warming anomalies over the NEP [*Zebiak*, 1993; *Latif and Grötzner*, 2000; *Okumura and Xie*, 2006; *Trzaska et al.*, 2007], the weakening of the Atlantic trade winds, and intensification of the equatorial westerlies [*Ruiz-Barradas et al.*, 2000] in which the classical Atlantic Niño and the SAOD described in this paper appear to be similar. It therefore seems plausible to argue that the signals of the SAOD are contained in some previous studies that were supposedly aimed at exploring the Atlantic Niño.

[44] However, in this study we have presented evidence to show that, while some warming episodes in the NEP/Atlantic Niño domain are solitary characteristics of the classical Atlantic Niño, others are associated with concurrent cooling anomaly of similar magnitude in the SWP off the Argentina-Uruguay-Brazil coast (that is, the SAOD). Because the present work is based on the diagnostic analysis of observational datasets, further dynamical studies through numerical experiments are necessary to improve our understanding on the structure, evolution, and teleconnections of the SAOD, and the mechanisms that differentiate it from the Atlantic Niño. These clarifications could provide a fresh perspective for investigating climate variability and for improved predictions, particularly over parts of Africa and the Americas.

[45] **Acknowledgments.** This work was jointly supported by the TWAS-CAS Postgraduate Fellowship and the 973 Program (2010CB950400) and NSFC Key Project (41030961). We are grateful to our colleagues at LASG, Institute of Atmospheric Physics, Chinese Academy of Sciences, Beijing, for useful comments during the course of the project and, to Dr Peter Knippertz and two anonymous reviewers for their constructive criticisms.

References

Adler, R. F., et al. (2003), The version 2 Global Precipitation Climatology Project (GPCP) monthly precipitation analysis (1979–present), *J. Hydrometeorol.*, *4*, 1147–1167, doi:10.1175/1525-7541(2003)004<1147:TVGPCP>2.0.CO;2.

Ajayamohan, R. S., and S. A. Rao (2008), Indian Ocean dipole modulates the number of extreme rainfall events over India in a warming environment, *J. Meteorol. Soc. Jpn.*, *86*, 245–252, doi:10.2151/jmsj.86.245.

Ashok, K., Z. Guan, and T. Yamagata (2001), Impact of the Indian Ocean dipole on the relationship between the Indian monsoon rainfall and ENSO, *Geophys. Res. Lett.*, *28*, 4499–4502, doi:10.1029/2001GL013294.

Ashok, K., Z. Guan, and T. Yamagata (2003), Influence of the Indian Ocean dipole on the Australian winter rainfall, *Geophys. Res. Lett.*, *30*(15), 1821, doi:10.1029/2003GL017926.

Bjerknes, J. (1969), Atmospheric teleconnections from the equatorial Pacific, *Mon. Weather Rev.*, *97*, 163–172, doi:10.1175/1520-0493(1969)097<0163:ATFTEP>2.3.CO;2.

Bretherton, C. S., C. Smith, and J. M. Wallace (1992), An intercomparison of methods for finding coupled patterns in climate data, *J. Clim.*, *5*, 541–560, doi:10.1175/1520-0442(1992)005<0541:AIOMFF>2.0.CO;2.

Chang, P., L. Ji, and H. Li (1997), A decadal climate variation in the tropical Atlantic Ocean from thermodynamic air-sea interactions, *Nature*, *385*, 516–518, doi:10.1038/385516a0.

Chiang, J. C. H., and D. J. Vimont (2004), Analogous Pacific and Atlantic meridional modes of tropical atmosphere-ocean variability, *J. Clim.*, *17*, 4143–4158, doi:10.1175/JCLI4953.1.

Colberg, F., and C. J. C. Reason (2007), Ocean model diagnosis of low-frequency climate variability in the South Atlantic region, *J. Clim.*, *20*, 1016–1034, doi:10.1175/JCLI4055.1.

Compagnucci, R. H., and M. B. Richman (2008), Can principal component analysis provide atmospheric circulation or teleconnection patterns?, *Int. J. Climatol.*, *28*, 703–726, doi:10.1002/joc.1574.

Ding, H., N. S. Keenlyside, and M. Latif (2010), Equatorial Atlantic interannual variability: Role of heat content, *J. Geophys. Res.*, *115*, C09020, doi:10.1029/2010JC006304.

Dommenget, D., and M. Latif (2002), A cautionary note on the interpretation of EOFs, *J. Clim.*, *15*, 216–225, doi:10.1175/1520-0442(2002)015<0216:ACNOTI>2.0.CO;2.

Enfield, D. B., A. M. Mestas-Nuñez, D. A. Mayer, and L. Cid-Serrano (1999), How ubiquitous is the dipole relationship in tropical Atlantic sea surface temperatures?, *J. Geophys. Res.*, *104*(C4), 7841–7848, doi:10.1029/1998JC900109.

Goddard, L., and S. J. Mason (2002), Sensitivity of seasonal climate forecasts to persisted SST anomalies, *Clim. Dyn.*, *19*, 619–632, doi:10.1007/s00382-002-0251-y.

Gordon, A. L. (1986), Interocean exchange of thermocline water, *J. Geophys. Res.*, *91*(C4), 5037–5046, doi:10.1029/JC091iC04p05037.

Guan, Z., and T. Yamagata (2003), The unusual summer of 1994 in East Asia: IOD teleconnections, *Geophys. Res. Lett.*, *30*(10), 1544, doi:10.1029/2002GL016831.

Haarsma, R. J., E. J. D. Campos, and F. Molteni (2003), Atmospheric response to South Atlantic SST dipole, *Geophys. Res. Lett.*, *30*(16), 1864, doi:10.1029/2003GL017829.

Haarsma, R. J., E. J. D. Campos, W. Hazeleger, C. Severijns, A. R. Piola, and F. Molteni (2005), Dominant modes of variability in the South Atlantic:

A study with a hierarchy of ocean-atmosphere models, *J. Clim.*, *18*, 1719–1735, doi:10.1175/JCLI3370.1.

Hu, Z., and B. Huang (2007), Physical processes associated with the tropical Atlantic SST gradient during the anomalous evolution in the southeastern ocean, *J. Clim.*, *20*, 3366–3378, doi:10.1175/JCLI4189.1.

Joly, M., and A. Voldoire (2010), Role of the Gulf of Guinea in the interannual variability of the West African monsoon: What do we learn from CMIP3 coupled simulations?, *Int. J. Climatol.*, *30*, 1843–1856.

Kalnay, E., et al. (1996), The NCEP/NCAR 40-year reanalysis project, *Bull. Am. Meteorol. Soc.*, *77*, 437–471, doi:10.1175/1520-0477(1996)077<0437:TNYRP>2.0.CO;2.

Lareef, Z., A. S. Rao, and T. Yamagata (2003), Modulation of Sri Lankan Maha rainfall by the Indian Ocean dipole, *Geophys. Res. Lett.*, *30*(2), 1063, doi:10.1029/2002GL015639.

Latif, M., and A. Grötzner (2000), The equatorial Atlantic oscillation and its response to ENSO, *Clim. Dyn.*, *16*, 213–218, doi:10.1007/s003820050014.

Li, J., and J. Wang (2003), A new North Atlantic Oscillation index and its variability, *Adv. Atmos. Sci.*, *20*, 661–676, doi:10.1007/BF02915394.

Li, Z. X. (2001), Thermodynamic air-sea interactions and tropical Atlantic SST dipole pattern, *Phys. Chem. Earth B*, *26*, 155–157.

Melice, J. L., and J. Servain (2003), The tropical Atlantic meridional SST gradient index and its relationships with the SOI, NAO and Southern Ocean, *Clim. Dyn.*, *20*, 447–464.

Monahan, A. H., J. C. Fyfe, M. H. P. Ambaum, D. B. Stephenson, and G. R. North (2009), Empirical orthogonal functions: The medium is the message, *J. Clim.*, *22*, 6501–6514, doi:10.1175/2009JCLI3062.1.

Nnamchi, H. C., and J. Li (2011), Influence of the South Atlantic Ocean dipole on West African summer precipitation, *J. Clim.*, *24*, 1184–1197, doi:10.1175/2010JCLI3668.1.

Okumura, Y., and S.-P. Xie (2006), Some overlooked features of tropical Atlantic climate leading to a new Niño-like phenomenon, *J. Clim.*, *19*, 5859–5874, doi:10.1175/JCLI3928.1.

Rayner, N. A., P. Brohan, D. E. Parker, C. K. Folland, J. J. Kennedy, M. Vanicek, T. Ansell, and S. F. B. Tett (2006), Improved analyses of changes and uncertainties in sea surface temperature measured in situ since the mid-nineteenth century: The HadSST2 dataset, *J. Clim.*, *19*, 446–469, doi:10.1175/JCLI3637.1.

Ruiz-Barradas, A., J. A. Carton, and S. Nigam (2000), Structure of interannual-to-decadal climate variability in the tropical Atlantic sector, *J. Clim.*, *13*, 3285–3297, doi:10.1175/1520-0442(2000)013<3285:SOITDC>2.0.CO;2.

Saji, N. H., B. N. Goswami, P. N. Vinayachandran, and T. Yamagata (1999), A dipole mode in the tropical Indian Ocean, *Nature*, *401*, 360–363, doi:10.1038/43854.

Servain, J. (1991), Simple climatic indices for the tropical Atlantic Ocean and some applications, *J. Geophys. Res.*, *96*(C8), 15,137–15,146, doi:10.1029/91JC01046.

Servain, J., and D. M. Legler (1986), Empirical orthogonal function analysis of tropical Atlantic sea surface temperature and wind stress: 1964–1979, *J. Geophys. Res.*, *91*(C12), 14,181–14,191, doi:10.1029/JC091iC12p14181.

Smith, T. M., R. W. Reynolds, T. C. Peterson, and J. Lawrimore (2008), Improvements to NOAA's historical merged land–ocean surface temperature analysis (1880–2006), *J. Clim.*, *21*, 2283–2296, doi:10.1175/2007JCLI2100.1.

Sterl, A., and W. Hazeleger (2003), Coupled variability and air-sea interaction in the South Atlantic Ocean, *Clim. Dyn.*, *21*, 559–571, doi:10.1007/s00382-003-0348-y.

Trzaska, S., A. W. Robertson, J. Farrara, and C. R. Mechoso (2007), South Atlantic variability arising from air-sea coupling: Local mechanisms and tropical-subtropical interactions, *J. Clim.*, *20*, 3345–3365, doi:10.1175/JCLI4114.1.

Venegas, S., L. Mysak, and D. Straub (1996), Evidence for interannual and interdecadal climate variability in the South Atlantic, *Geophys. Res. Lett.*, *23*, 2673–2676, doi:10.1029/96GL02373.

Venegas, S. A., L. A. Mysak, and D. N. Straub (1997), Atmosphere-ocean coupled variability in the South Atlantic, *J. Clim.*, *10*, 2904–2920, doi:10.1175/1520-0442(1997)010<2904:AOCVIT>2.0.CO;2.

Weare, B. C. (1977), Empirical orthogonal analysis of Atlantic Ocean surface temperatures, *Q. J. R. Meteorol. Soc.*, *103*, 467–478, doi:10.1002/qj.49710343707.

Weijer, W., W. P. M. De Ruijter, A. Sterl, and S. S. Drijfhout (2002), Response of the Atlantic overturning circulation to South Atlantic sources of buoyancy, *Global Planet. Change*, *34*, 293–311, doi:10.1016/S0921-8181(02)00121-2.

Woodruff, S. D., R. J. Slutz, R. L. Jenne, and P. M. Steurer (1987), A comprehensive ocean–atmosphere data set, *Bull. Am. Meteorol. Soc.*, *68*, 1239–1250, doi:10.1175/1520-0477(1987)068<1239:ACOADS>2.0.CO;2.

Zebiak, S. E. (1993), Air–sea interaction in equatorial Atlantic region, *J. Clim.*, *6*, 1567–1586, doi:10.1175/1520-0442(1993)006<1567:AIITEA>2.0.CO;2.

R. N. C. Anyadike, Department of Geography, University of Nigeria, Nsukka 410001, Nigeria.

J. Li and H. C. Nnamchi, State Key Laboratory of Numerical Modelling for Atmospheric Sciences and Geophysical Fluid Dynamics, Institute of Atmospheric Physics, Chinese Academy of Sciences, Beijing 100029, China. (ljp@lasg.iap.ac.cn)